THE JOURNAL OF PHYSICAL CHEMISTRY C

Article

Cite This: J. Phys. Chem. C 2018, 122, 9134−9140

pubs.acs.org/JPCC

Signal Enhancement from Tunable SERS Substrates: Design and Demonstration of Multiple Regimes of Enhancement

Deepak Ranjan Nayak,[†] Navakanta Bhat,[†] Murugesan Venkatapathi,[‡] and Siva Umapathy*[,§,∥]

[†]Centre for Nano Science and Engineering, [‡]Computational & Statistical Physics Laboratory, Department of Computational & Data Sciences, [§]Department of Inorganic and Physical Chemistry, and [∥]Department of Instrumentation and Applied Physics, Indian Institute of Science, Bangalore 560012, India

Supporting Information

ABSTRACT: The interaction between plasmonic nanoparticle and substrate is of utmost importance for optimal design of surface-enhanced Raman spectroscopy (SERS) substrates. Substrates can either quench or enhance the strength of the localized plasmon resonance of nanoparticles depending on the optical properties. The substrate optical properties were modified by introducing different dielectric films between silver nanoparticle and silicon base substrates. The thickness of the films was varied over a large range (5−200 nm) to observe SERS enhancement because of nonradiative and radiative interactions of the plasmons and the substrate. Energy transfer between the plasmons and the polarization charges in Si was observed for a film thickness of less than 10 nm where SERS intensity followed the permittivity trend of the spacer film. As the spacer thickness increases beyond 40 nm, the effect of Si base substrate subsides and the enhancement/quenching of the SERS signals exhibit an oscillatory behavior with the thickness of the film. The extent of enhancement and quenching can be tuned by optical property of substrate and the excitation wavelength of choice.

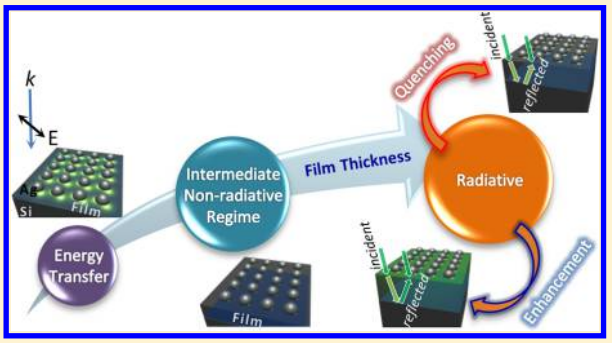

1. INTRODUCTION

Surface-enhanced Raman spectroscopy (SERS) is a sensitive technique for the detection of trace levels of analytes with a unique spectral signature. The method involves near-field enhancement from a metal nanostructure, thereby amplifying the typical normal Raman signal of analyte molecule adsorbed on the metal surface by millions of orders of magnitude.[1] This near-field enhancement arises because of collective oscillation of the free surface electrons of metal which is termed as localized surface plasmon resonance (LSPR). A significant contribution to the strength and position of the LSPR mode comes from the media surrounding the nanoparticle. LSPR of nanoparticle in a homogenous medium has been modeled and the results are well-established with respect to SERS.[2,3] However, modeling a nanoparticle in heterogeneous media (nanoparticle on a substrate) has been a challenge. Several reports have highlighted various substrate-associated effects that influence LSPR enhancement. In general, there are two types of effects of substrates, namely, nonradiative and radiative. To achieve maximum enhancement, it is important to understand these effects by experiments and numerical calculations.

Establishing the substrate effects on LSPR because of nonradiative and radiative interactions has led to intricate numerical models and computationally expensive simulations.[4−10] Plasmon resonance mode of the metal nanoparticle on a substrate may shift and split depending on the substrate optical property.[9,11,12] This is due to the nonradiative interaction between the nanoparticle and the substrate. For example, oscillating plasmons induce an image on the substrate. The image couples to the plasmons causing significant shift in the resonance mode energy compared with their free-space energy. Such image charge formation has been reported to be proportional to the permittivity of the substrate.[13] Interestingly, previous reports have correlated the permittivity of the substrate with the resonance strength of plasmonic nanoparticles.[9,14−17] Some of the reports discuss image charge coupling between the metal/semiconducting substrate and plasmonic nanoparticle separated by a thin spacer film.[15,18−23] In most of the studies, spacer layer permittivity is not accounted for.

It is also known that the radiative effect from the substrate can either enhance or quench the resonance strength.[14,24−26] This effect originates because of the change in the electric field amplitude of the incident wave after reflection or refraction at a surface. Hence, the nanoparticle experiences electric field amplitude which is either higher or lower than the amplitude of the wave originating from the source. The quenching, in this report, refers to the decrease in electric field amplitude due to electric field superposition rather than quenching of fluorescence signal in SERS due to the adsorption of fluorescent

Received: February 22, 2018
Revised: April 5, 2018
Published: April 6, 2018

DOI: 10.1021/acs.jpcc.8b01814
J. Phys. Chem. C 2018, 122, 9134−9140

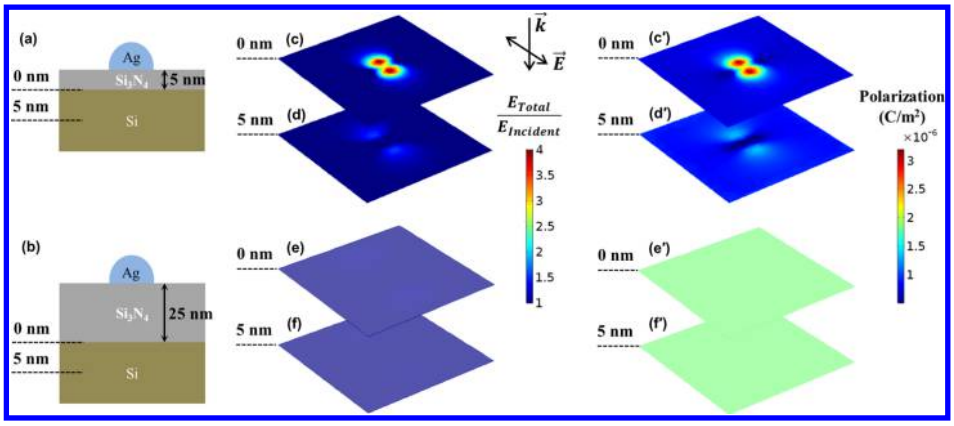

Figure 1. Schematic (a,b) represent the substrates with 5 and 25 nm Si_3N_4 spacers. Dotted lines in the schematic represent the surfaces for which electric field enhancement and polarization have been plotted in the figures (c−f,c′−f′). Field enhancement at the (c) Si_3N_4−Si interface and (d) 5 nm below the interface for substrate with 5 nm Si_3N_4 spacer layer. Panels (e,f) correspond to the same with 25 nm Si_3N_4 spacer layer. Polarization profile at the (a′) Si_3N_4−Si interface and (b′) 5 nm below the interface for substrate with 5 nm Si_3N_4 spacer layer. Panels (c′,d′) correspond to the same with 25 nm Si_3N_4 spacer layer.

molecules on the metal. The radiative effect has direct implication on the SERS activity.[25−30] However, more complex effects are expected when an insulating spacer film is inserted between the nanoparticles and the base substrate. The effect from the substrate (base substrate and spacer combined) is a function of the thickness and permittivity of the spacer film which dictates the relative contribution from both nonradiative and radiative interactions. Modulating these interactions between the nanoparticle and the substrate has direct influence on the LSPR and thus on the SERS activity of the substrates. Radiative interaction has been studied independently.[15,31−34] Although these reports are comprehensive, the radiative effect with respect to substrates and films of different permittivity has not been taken into account. These aspects are necessary as the permittivity-dependent image charge (nonradiative part) would also contribute to the total enhancement.

Our earlier report has established a correlation between the SERS enhancement and LSPR peak shift due to energy transfer.[35] Energy transfer occurs between the plasmons and the polarization charges in the silicon base substrate, when an interleaving ultrathin dielectric film (<∼10 nm) produces a layer of large polarization at the film-substrate boundary. With the increasing spacer thickness (>10 nm), the LSPR strength and positions are modulated only by the permittivity of the spacer layer with little influence from the substrate. Here, we observe that the radiative effect becomes dominant as the thickness increases beyond ∼40 nm. We propose a model in conjunction with the experimental data and predict gain in SERS substrates by taking energy transfer and nonradiative and radiative interactions into account. The analytical model is computationally inexpensive and provides additional insights into the physics by decoupling the substrate effects into different regimes. To the best of our knowledge, it is the first report which brings all possible substrate effects in a simple analytical model and thus demonstrates the multiple regimes of enhancement facilitating the control of wavelength tunability and intensity enhancement. This would provide deep insights into the plasmonic enhancement in stacked plasmonic substrates for various applications.[36−38]

2. THEORETICAL METHODS

In this section, the simulation results along with the assumptions in the analytical model have been discussed. An analytical model is formulated to decouple different substrate effects which is otherwise not possible using numerical tools. The following discussion pertains to a simple model of a nanoparticle on a substrate separated by a spacer film of varying thickness (refer Supporting Information for detailed description). The shape of the nanoparticles on the substrates is approximated as a hemisphere, which has three LSPR modes when excited with a plane-wave polarized along the plane (Figure S3). These modes undergo shift because of the substrate effect (Figure S5). The lowest energy dipolar mode has been modeled for enhancement calculation.

Computation was carried out using COMSOL Multiphysics 4.4 (FEM based solver). The details of the simulation domain and equations are provided in the Supporting Information. COMSOL simulations have been carried out for two models, a substrate with a 5 nm spacer (Figure 1a) and a substrate with a 25 nm spacer (Figure 1b). It is observed that the enhanced electric field of the nanoparticle extends through the spacer till the spacer−Si interface (Figure 1c). The field still remains relatively intense till 5 nm deep into the volume of the base Si substrate (Figure 1d). Hence, it can be inferred that the incident electromagnetic wave completely polarizes the metal nanoparticle which in turn polarizes the base Si substrate. The polarization not only happens at the spacer−Si interface (Figure 1c′) but also deep into the volume (Figure 1d′). This phenomenon is absent in the case of 25 nm spacer layer. It is intuitive that the spacer−Si interface is at a distance of 25 nm which is far away from the near-field zone of the nanoparticle and does not experience the enhanced field (Figure 1e,f) and thus does not promote any polarization in the Si substrate (Figure 1e′,f′).

Therefore, the magnitude of polarization in the Si volume greatly depends on the spacer film thickness (d). The coupling between the oscillating plasmons and the polarization charges in the semiconducting substrate is termed as energy transfer. The effect is also observed in Figure 2 (left axis) from the shift in the LSPR peak position with respect to the spacer thickness. There is a definite coupling involved between the nanoparticle and Si substrate for the thinner film which causes red shift in LSPR compared with the nanoparticle on a bulk film (equivalent to spacer thickness > ∼10 nm). For the thicker film, however, the effect vanishes and the LSPR shift depends only on the permittivity of the film. In the simulation, film

DOI: 10.1021/acs.jpcc.8b01814
J. Phys. Chem. C 2018, 122, 9134−9140

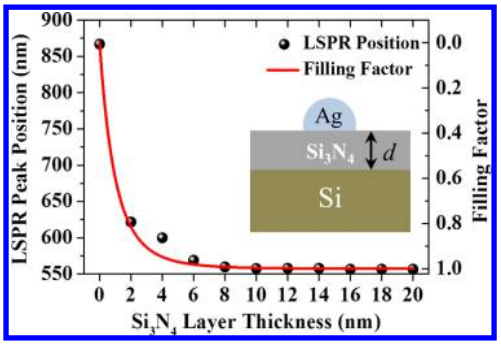

Figure 2. Comparison of filling factor (eq 1) and LSPR peak position of 14 nm Ag on varying Si_3N_4 spacer thickness.

permittivity has been kept constant to bring out the effect of thickness alone. The description of energy transfer here is purely based on the extent of enhanced near field which is different from the explanation based on band structures of material as reported elsewhere.[39,40]

It is evident that the LSPR peak position is solely modulated by the coupling between the plasmon and its image on the spacer−substrate (Si_3N_4−Si) interface for thin spacers. This calls for an effective permittivity model which reduces the problem from nanoparticle−spacer−Si to nanoparticle-effective substrate. The effective substrate optical property would consist of both the permittivity of the spacer and a fraction of the permittivity of the base substrate (Si). Later, the nanoparticle-effective substrate problem is solved by image charge model.

2.1. Energy Transfer and Nonradiative Model. The effective substrate model in eq 1 has been adapted from the Maxwell Garnett's effective medium approximation.[41] Effective medium approximation has been modified to take inclusions into account which are finite in two or three dimensions (e.g., cylinder and sphere).[42] This model is approximated for the spacer film which is finite in one dimension. The equation incorporates permittivity of the spacer film (ε_f) and Si (ε_{Si}) to calculate effective substrate permittivity (ε_{effs}).

The filling factor (eq 2), in essence, defines the ratio of the volume of the spacer and the base Si substrate. Because the elements are optically infinite in two dimensions, the thickness ratio is an appropriate measure of the filling factor. The numerator of eq 2 takes into account the thickness of the spacer, and the denominator represents the thickness of the base substrate. The thickness of the base substrate does not represent the physical thickness (thickness of a Si wafer) but the extent of near-field radiation of the plasmonic nanoparticle in the substrate. The radiation is modeled by a power function. The term l^{-6} represents the decay of near field from the plasmonic nanoparticle as a function of distance (l). The integration assumes that the dipole is placed at the centre of the nanoparticle ($a/2$, where a is the radius) to avoid singularity. A schematic of the integration method is provided in the Supporting Information (Figure S6) for clarity.

$$\frac{\varepsilon_{effs}(\lambda) - \varepsilon_{Si}(\lambda)}{\varepsilon_{effs}(\lambda)} = f\left(\frac{\varepsilon_f(\lambda) - \varepsilon_{Si}(\lambda)}{\varepsilon_f(\lambda)}\right) \quad (1)$$

$$f = \frac{\int_{a/2}^{d+a/2} \frac{1}{l^6}\,dl}{\int_{a/2}^{\infty} \frac{1}{l^6}\,dl} \quad (2)$$

The filling factor (f) ranges from 0 to 1 corresponding to pure Si permittivity to pure spacer film permittivity. Interestingly, the trend of the filling factor matches the LSPR shift when the integration is carried out over the sixth power of distance (Figure 2, right-axis). Such coupling, which depends on the sixth power of distance, is observed in the case of dipole−dipole coupling indicating energy transfer. The energy-transfer process is prominent for thin spacer layers and falls as $1/d^6$ as the spacer thickness (d) increases.

The absorption cross section (C_{abs}) from polarizability (α) for a hemisphere on substrate has been modeled earlier[4,5] and it has been modified in our previous work.[35] The formulation takes into account the permittivities of the metal nanoparticle (ε_{Ag}), medium (ε_m) and effective substrate permittivity (ε_{effs}) to calculate B_{11}. The size factor (sf, eq 4) has been introduced in eq 3 to account for red shift due to the increase in the size of the nanoparticle.[43] Volume polarizability (eq 5) is used for the calculation of absorption cross section in eq 6. It is imperative to note that the model predicts only the nonradiative nature of interaction of nanoparticle with the substrate for relatively thicker film (as $\varepsilon_{effs} = \varepsilon_f$ when $f = 1$).

$$B_{11} = \frac{(\varepsilon_m + \varepsilon_{effs})(\varepsilon_m - \varepsilon_{Ag})}{2\varepsilon_m(sf \times 2\varepsilon_m + sf \times 3\varepsilon_{effs} + \varepsilon_{Ag})} \quad (3)$$

$$sf = 0.83 + \frac{12}{5}x^2; \qquad x = k \times 2a; \qquad k = \frac{2\pi}{\lambda} \quad (4)$$

$$\alpha = -4\pi\varepsilon_{effs}a^3B_{11} \quad (5)$$

$$C_{abs} = k\ \mathrm{Im}[\alpha] \quad (6)$$

2.2. Radiative Model. In the energy transfer and nonradiative regime, the film thickness is optically small to contribute any considerable phase change in the reflected electric field. The phase change becomes more prominent for thicker films where the radiative effect prevails. The radiative part does not result in peak shift of the LSPR modes but contributes to the amplitude, whereas nonradiative interactions causes peak shift and amplitude modulation. Hence, the Fresnel coefficient was calculated for the substrates to account for radiative interaction based on thin film interference. Fresnel equations predict an enhancement of the electric field amplitude when an electromagnetic wave passes from a medium with high refractive index to a medium with low refractive index. Fresnel coefficients have been formulated for multilayered films case by taking the superposition of the incident and reflected waves.[44] In the discussed experiments, the excitation is perpendicular to the substrate surface and polarization parallel to it. The Fresnel reflection coefficient (R) for the said conditions reduces to eq 7. The reflection coefficients at the interface of the medium and film (r_{12}) and at the interface of the film and Si (r_{23}) with phase factor (δ) are used for the calculations (eq 8). The refractive index of the medium (n_m), film (n_f), and Si (n_s) are used to calculate the reflection coefficients and phase factors.

$$R = \frac{r_{12} + r_{23}\exp(-2i\delta)}{1 + r_{12}r_{23}\exp(-2i\delta)}; \qquad \text{intensity} = (1 + R)^2 \quad (7)$$

DOI: 10.1021/acs.jpcc.8b01814
J. Phys. Chem. C 2018, 122, 9134−9140

$$r_{12} = \frac{n_m - n_f}{n_m + n_f}; \qquad r_{23} = \frac{n_f - n_s}{n_f + n_s};$$
$$\delta = \frac{2\pi}{\lambda} n_f d \tag{8}$$

The nanoparticles experience electric field which is $1 + R$ factor of the incident field. Thus, the enhancement of the substrates gets modulated by $(1 + R)^2$ which represents the intensity. One of such results is provided in Figure 3 for the

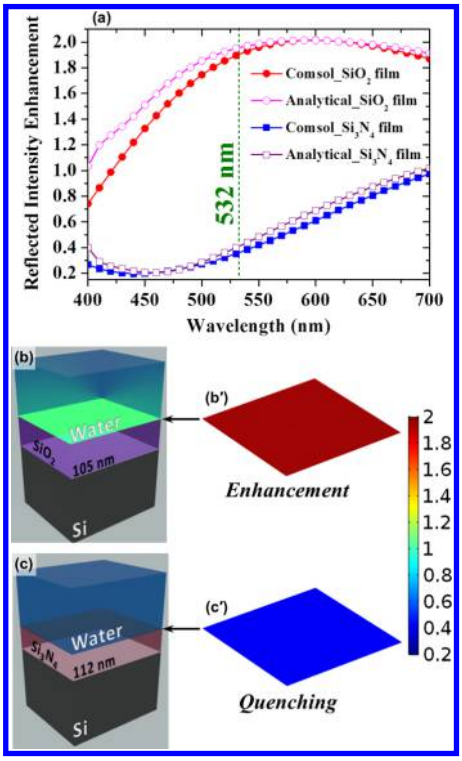

Figure 3. (a) Intensity enhancement at the water−spacer interface for substrates with 105 nm SiO_2 and 112 nm Si_3N_4 spacer. Intensity calculated from COMSOL and the analytical model have been compared. (b,c) Schematic of the substrates and the interface in discussion. (b′,c′) Surface plot of intensity at the interfaces.

demonstration of the effect. Substrates with 105 nm SiO_2 and 112 nm Si_3N_4 spacers have been opted because of the stark difference in their enhancement and quenching property, respectively. Figure 3a compares the intensity enhancement (E-field^2) at the water−spacer interface for both substrates using COMSOL and the analytical model (eq 7). The schematic of the substrate and the corresponding interface is shown in Figure 3b,c. It is evident that the substrate with SiO_2 enhances (Figure 3b′), whereas the substrate with Si_3N_4 quenches (Figure 3c′) at 532 nm. It is evident from this example that the radiative and nonradiative effects can be opposite in nature. Si_3N_4 has higher permittivity than SiO_2 which results in a stronger image charge formation (strong enhancement) but the thickness of the film results in quenching.

2.3. Complete Analytical Model. The total resonance strength can be expressed as in eq 9 which incorporates both nonradiative and radiative effects. The nonradiative effect captures the red shift and amplitude modulation in LSPR (Figure S5) with increasing permittivity.[12] The radiative effect captures the amount of near-field enhancement due to the total electric field at the nanoparticle−dielectric interface. It is valid to formulate eq 9 as $(1 + R)^2$ is a dimensionless quantity, and both factors in the equation represent second power of the electric field.

The relative gain for the substrates is formulated as the ratio of the resonance strength of the substrates to a specific (reference) substrate.

$$\text{Resonance strength} = C_{abs}(1 + R)^2 \tag{9}$$

$$\text{Relative gain} = \frac{[C_{abs}(1 + R)^2]_{substrate}}{[C_{abs}(1 + R)^2]_{reference}} \tag{10}$$

Individual contribution from nonradiative and radiative parts can be calculated by using the equations given below

$$(\text{Relative gain})_{non\text{-}radiative} = \frac{[C_{abs}]_{substrate}}{[C_{abs}]_{reference}} \tag{11}$$

$$(\text{Relative gain})_{radiative} = \frac{[(1 + R)^2]_{substrate}}{[(1 + R)^2]_{reference}} \tag{12}$$

Formulation of analytical models has aided in decoupling the substrate effects more efficiently through eqs 11 and 12 without resorting to computationally expensive numerical tools. The subsequent section will focus on verification of the analysis through experiments. For clarity, the equations presented above have been grouped according to their contribution to different effects in Figure S7.

3. EXPERIMENTAL METHODS

Different thicknesses of SiO_2 films were thermally grown (ET-6000, FirstNano oxidation furnace) and Si_3N_4 films were deposited by low-pressure chemical vapor deposition (ET-6000, FirstNano LPCVD furnace) process on a pristine Si⟨100⟩ wafer. The refractive index and thickness of the films were measured by spectroscopic ellipsometry (M200U, J.A. Woollam Co.) with the models and methods described in the Supporting Information. Validation for the thickness for few of the films was done using scanning electron microscopy (SEM) (Figure S9). SERS substrates were fabricated by the deposition of ∼5 nm of the silver film on the prefabricated substrates by dc magnetron sputtering (Tecport). Sputtering parameters were controlled to obtain similar (11 ± 4 nm) nanoparticle distribution on all substrates.

SERS characterization was carried out with 100 mM pyridine solution with 532 nm excitation using LabRAM HR800 equipped with 1800 grooves/mm grating. Spectra were acquired for 1 s acquisition using 50× (0.5 NA) objective with ∼5 mW power at the sample. All SERS spectra were collected by focusing the laser on the substrate through the analyte solution.

4. RESULTS AND DISCUSSION

To verify the analytical and numerical models, SERS substrates were fabricated by depositing different thickness of SiO_2 and Si_3N_4 film on Si and subsequently sputtering Silver. The thin silver film formed islands because of the Volmer−Weber growth mode.[45] The dispersion curves (Figure S8) for the dielectric films were obtained from ellipsometry and the method of calculation is provided in the Supporting Information. Representative nanoparticle distribution on the substrate with SiO_2 and Si_3N_4 films are shown in Figure 4. The nanoparticle distribution remains same irrespective of the film

DOI: 10.1021/acs.jpcc.8b01814
J. Phys. Chem. C 2018, 122, 9134−9140

thickness for all the substrates with SiO_2 spacers. The same has also been observed for Si_3N_4.

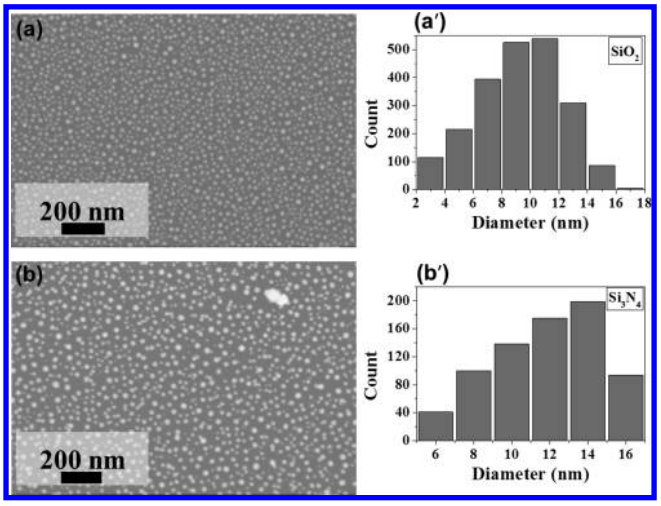

Figure 4. SEM images of substrates with (a) SiO_2 and (b) Si_3N_4 films and the corresponding nanoparticle distribution in (a′,b′).

Pyridine was chosen as the test analyte on all substrates. The Raman peaks at 1007 and 1036 cm^{-1} correspond to ring breathing and symmetric ring deformation modes, respectively.[46] Multiple SERS spectra were recorded for each substrate and the baseline correction was carried out. The spectra were averaged and the intensity for 1036 cm^{-1} peak with standard error has been plotted in Figure 5a corresponding to the substrates with Si_3N_4 and SiO_2 films. An example of the processing method with the raw data is provided in Figure S10.

The experimental relative gain for different SiO_2 substrates was calculated by taking the ratio of the SERS intensity of a substrate to that of the substrate with the 150 nm SiO_2 film. The experimental and analytical gains (eq 10) have been plotted in the Figure 5b for substrates with the SiO_2 spacer film. Similarly, the gains for the substrates with Si_3N_4 have been plotted in Figure 5c. The enhancement trends observed in the substrates with the SiO_2 and Si_3N_4 spacer are reasonably predicted by the analytical model (eq 10).

The individual contributions from the nonradiative and radiative effects, using eqs 11 and 12, have been plotted in Figure 5b′,c′. Figure 5b′,c′ correspond to the substrates with SiO_2 and Si_3N_4 spacers, respectively. The substrate with a 150 nm spacer was taken as the reference substrate in all calculations. This is in good agreement with the assumptions made in formulating the analytical models. It is clearly observed that the radiative effect modulates the SERS intensity for thicker film whereas the nonradiative part remains nearly constant. The constant nonradiative effect is due to the similar permittivity value for thicker films (Figure S8).

The above discussions point the complexity involved in predicting efficacy of the SERS substrates which strongly depend on the permittivity and spacer thickness. These effects can also be demonstrated across substrates with different spacers. The SERS intensity obtained from the 150 nm Si_3N_4 spacer substrate was scaled with respect to the 150 nm SiO_2 spacer substrate. The factor was used to scale the gain plot in Figure 5c to obtain Figure 6 which represents the performance of the Si_3N_4 spacer substrate.

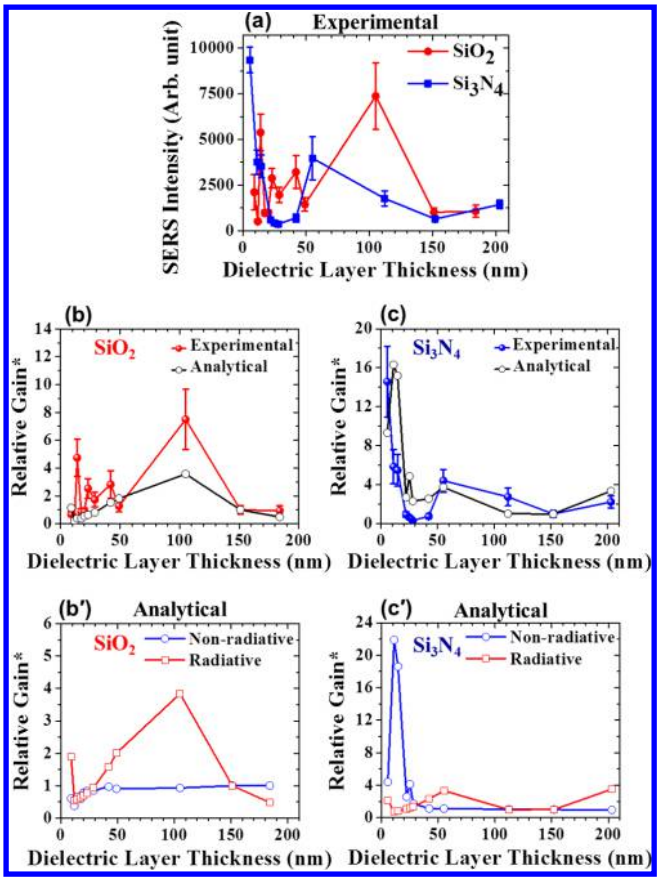

Figure 5. (a) Experimental SERS intensity from substrates with various spacers. Experimental and computational gain obtained from substrates with (b) SiO_2 and (c) Si_3N_4 films. The gains are calculated relative to the substrate with a 150 nm spacer substrate. Effects of radiative and nonradiative interactions have been plotted separately for substrates with (b′) SiO_2 and (c′) Si_3N_4 films corresponding to the result from the analytical model in (bc) $*(I/I_{150nm})$.

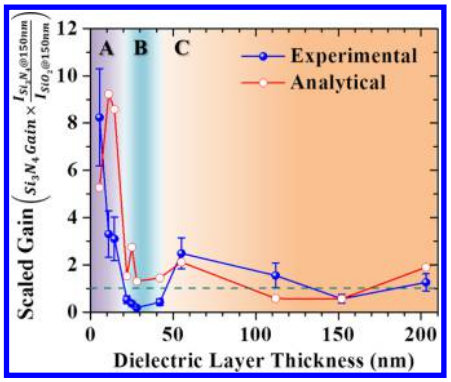

Figure 6. Enhancement observed in the substrates with Si_3N_4 films with respect to the substrates with SiO_2. Green dotted line indicates the boundary between substrate's enhancing or quenching property. Three different regimes (A-energy transfer, B-intermediate nonradiative, and C-radiative) of substrate effects are approximately marked with different color shades.

The oscillations around the dotted line in Figure 6 suggest that the Si_3N_4 spacer substrates enhance (>1) as well as quench (<1) for various thicknesses with respect to the SiO_2 spacer substrate. As per the trend, the total nanoparticle−substrate interaction can be divided into three important regimes. The energy-transfer regime (A) always enhances with respect to the

DOI: 10.1021/acs.jpcc.8b01814
J. Phys. Chem. C 2018, 122, 9134−9140

permittivity of the spacer layer. Energy transfer screened by the permittivity of the spacer layer is sufficient to explain the phenomenon. An intermediate nonradiative regime (B) exists below ∼40 nm because of the Coulombic interaction of NP with the film and changes with the changing permittivity of the film. As the thickness increases, the filling factor (eq 2) approaches 1, signifying no contribution from the Si base substrate. The results obtained from eq 6 are only dependent on the experimental permittivity values of the spacers (Figure S8). In the higher thickness regime (C), permittivity does not vary with respect to the thickness of spacers resulting in similar coulombic interaction among substrates. The only factor responsible for modulating the intensity is the radiative effect as described in eq 7 and observed from Figure 5b′,c′.

5. CONCLUSIONS

The experimental and analytical study has clearly indicated three possible effects which are observed experimentally and through analytical models. Energy transfer causes SERS enhancement which is strongly dependent on the spacer thickness and permittivity and lasts up to 10 nm thickness. The resonance strength of the nanoparticle is weakly affected by the base substrate above 10 nm spacer layer thickness. The contribution from the radiative effect is substantial and subdues the other effects for higher spacer film thickness (>∼40 nm). Hence, the radiative part alone is sufficient to predict an average behavior of resonance strength in case of thicker spacer layers. This analysis highlights the importance of selecting materials with suitable optical properties to obtain enhancement of SERS for a specific wavelength.

■ ASSOCIATED CONTENT

Supporting Information

The Supporting Information is available free of charge on the ACS Publications website at DOI: 10.1021/acs.jpcc.8b01814.

Computational methods and results, integration limit of filling factor, experimental dispersion curve, Raman data processing, gain scaling, additional comments (PDF)

■ AUTHOR INFORMATION

Corresponding Author

*E-mail: siva.umapathy@gmail.com. Phone: 91-80-22932595/23601234. Fax: 91-80-23601552/23600803.

ORCID

Deepak Ranjan Nayak: 0000-0002-0436-6267

Siva Umapathy: 0000-0002-8538-5004

Author Contributions

The manuscript was written through contributions of all authors. All authors have given approval to the final version of the manuscript.

Notes

The authors declare no competing financial interest.

■ ACKNOWLEDGMENTS

The research was supported by Department of Electronics and Information Technology (Deity), Govt. of India under CEN (Centre of Excellence in Nanoelectronics). Part of the research has been funded by Defence Research and Development Organisation (DRDO), Ministry of Defence. S.U. acknowledges the J. C. Bose Fellowship funding from the Department of Science and Technology (DST), Govt. of India.

■ REFERENCES

(1) Le Ru, E.; Blackie, E.; Meyer, M.; Etchegoin, P. G. Surface Enhanced Raman Scattering Enhancement Factors: A Comprehensive Study. *J. Phys. Chem. C* **2007**, *111*, 13794−13803.

(2) Zhao, J.; Pinchuk, A. O.; McMahon, J. M.; Li, S.; Ausman, L. K.; Atkinson, A. L.; Schatz, G. C. Methods for Describing the Electromagnetic Properties of Silver and Gold Nanoparticles. *Acc. Chem. Res.* **2008**, *41*, 1710−1720.

(3) Moskovits, M. Surface-Enhanced Spectroscopy. *Rev. Mod. Phys.* **1985**, *57*, 783.

(4) Wind, M. M.; Vlieger, J.; Bedeaux, D. The Polarizability of a Truncated Sphere on a Substrate I. *Phys. A* **1987**, *141*, 33−57.

(5) Wind, M. M.; Bobbert, P. A.; Vlieger, J.; Bedeaux, D. The Polarizability of a Truncated Sphere on a Substrate II. *Phys. A* **1987**, *143*, 164−182.

(6) Ruppin, R. Surface Modes and Optical Absorption of a Small Sphere above a Substrate. *Surf. Sci.* **1983**, *127*, 108−118.

(7) Ruppin, R. Optical Absorption by a Small Sphere above a Substrate with Inclusion of Nonlocal Effects. *Phys. Rev. B: Condens. Matter Mater. Phys.* **1992**, *45*, 11209.

(8) Eremin, Y.; Orlov, N. Simulation of Light Scattering from a Particle upon a Wafer Surface. *Appl. Opt.* **1996**, *35*, 6599−6604.

(9) Hutter, T.; Elliott, S. R.; Mahajan, S. Interaction of Metallic Nanoparticles with Dielectric Substrates: Effect of Optical Constants. *Nanotechnology* **2013**, *24*, 035201.

(10) Wu, Y.; Nordlander, P. Finite-difference Time-domain Modeling of the Optical Properties of Nanoparticles near Dielectric Substrates. *J. Phys. Chem. C* **2009**, *114*, 7302−7307.

(11) Albella, P.; Garcia-Cueto, B.; González, F.; Moreno, F.; Wu, P. C.; Kim, T.-H.; Brown, A.; Yang, Y.; Everitt, H. O.; Videen, G. Shape Matters: Plasmonic Nanoparticle Shape Enhances Interaction with Dielectric Substrate. *Nano Lett.* **2011**, *11*, 3531−3537.

(12) Kadkhodazadeh, S.; Christensen, T.; Beleggia, M.; Mortensen, N. A.; Wagner, J. B. The Substrate Effect in Electron Energy-loss Spectroscopy of Localized Surface Plasmons in Gold and Silver Nanoparticles. *ACS Photonics* **2017**, *4*, 251−261.

(13) Knight, M. W.; Wu, Y.; Lassiter, J. B.; Nordlander, P.; Halas, N. J. Substrates Matter: Influence of an Adjacent Dielectric on an Individual Plasmonic Nanoparticle. *Nano Lett.* **2009**, *9*, 2188−2192.

(14) Venkatapathi, M.; Tiwari, A. K. Radiative and Non-radiative Effects of a Substrate on Localized Plasmon Resonance of Particles. *J. Appl. Phys.* **2012**, *112*, 013529.

(15) Wang, T.; Zhang, Z.; Liao, F.; Cai, Q.; Li, Y.; Lee, S.-T.; Shao, M. The Effect of Dielectric Constants on Noble Metal/Semiconductor SERS Enhancement: FDTD Simulation and Experiment Validation of Ag/Ge and Ag/Si Substrates. *Sci. Rep.* **2014**, *4*, 4052.

(16) Glembocki, O. J.; Rendell, R. W.; Alexson, D. A.; Prokes, S. M.; Fu, A.; Mastro, M. A. Dielectric-substrate-induced Surface-enhanced Raman Scattering. *Phys. Rev. B: Condens. Matter Mater. Phys.* **2009**, *80*, 085416.

(17) Vernon, K. C.; Funston, A. M.; Novo, C.; Gómez, D. E.; Mulvaney, P.; Davis, T. J. Influence of Particle−substrate Interaction on Localized Plasmon Resonances. *Nano Lett.* **2010**, *10*, 2080−2086.

(18) Ciracì, C.; Hill, R. T.; Mock, J. J.; Urzhumov, Y.; Fernández-Domínguez, A. J.; Maier, S. A.; Pendry, J. B.; Chilkoti, A.; Smith, D. R. Probing the Ultimate Limits of Plasmonic Enhancement. *Science* **2012**, *337*, 1072−1074.

(19) Mahdy, M. R. C.; Zhang, T.; Danesh, M.; Ding, W. Substrate and Fano Resonance Effects on the Reversal of Optical Binding Force between Plasmonic Cube Dimers. *Sci. Rep.* **2017**, *7*, 6938.

(20) Thomas, A.; Trivedi, R.; Dhawan, A. Plane Wave Scattering from a Plasmonic Nanowire Array Spacer-separated from a Plasmonic Film. *Mater. Res. Express* **2016**, *3*, 065004.

(21) Powell, A. W.; Smith, J. M. Mediating Fano Losses in Plasmonic Scatterers by Tuning the Dielectric Environment. *Appl. Phys. Lett.* **2016**, *109*, 121107.

(22) Okamoto, T.; Yamaguchi, I. Optical Absorption Study of the Surface Plasmon Resonance in Gold Nanoparticles Immobilized onto

DOI: 10.1021/acs.jpcc.8b01814
J. Phys. Chem. C 2018, 122, 9134−9140

a Gold Substrate by Self-assembly Technique. *J. Phys. Chem. B* **2003**, *107*, 10321−10324.
(23) Nordlander, P.; Prodan, E. Plasmon Hybridization in Nanoparticles near Metallic Surfaces. *Nano Lett.* **2004**, *4*, 2209−2213.
(24) Auguié, B.; Bendaña, X. M.; Barnes, W. L.; de Abajo, F. J. G. Diffractive Arrays of Gold Nanoparticles near an Interface: Critical Role of the Substrate. *Phys. Rev. B: Condens. Matter Mater. Phys.* **2010**, *82*, 155447.
(25) Huang, K.; Pan, W.; Zhu, J. F.; Li, J. C.; Gao, N.; Liu, C.; Ji, L.; Yu, E. T.; Kang, J. Y. Asymmetric Light Reflectance from Metal Nanoparticle Arrays on Dielectric Surfaces. *Sci. Rep.* **2015**, *5*, 18331.
(26) Jayawardhana, S.; Rosa, L.; Juodkazis, S.; Stoddart, P. R. Additional Enhancement of Electric Field in Surface-enhanced Raman Scattering Due to Fresnel Mechanism. *Sci. Rep.* **2013**, *3*, 2335.
(27) Jelmakas, E.; Kadys, A.; Malinauskas, T.; Paipulas, D.; Dobrovolskas, D.; Dmukauskas, M.; Selskis, A.; Juodkazis, S.; Tomašiūnas, R. A Systematic Study of Light Extraction Efficiency Enhancement Depended on Sapphire Flipside Surface Patterning by Femtosecond Laser. *J. Phys. D: Appl. Phys.* **2015**, *48*, 285104.
(28) Woods, D. A.; Bain, C. D. Total Internal Reflection Raman Spectroscopy. *Analyst* **2012**, *137*, 35−48.
(29) Bottomley, A.; Ianoul, A. Reflection and Absorption Spectra of Silver Nanocubes on a Dielectric Substrate: Anisotropy, Angle, and Polarization Dependencies. *J. Phys. Chem. C* **2014**, *118*, 27509−27515.
(30) Chou, A.; Jaatinen, E.; Buividas, R.; Seniutinas, G.; Juodkazis, S.; Izake, E. L.; Fredericks, P. M. SERS Substrate for Detection of Explosives. *Nanoscale* **2012**, *4*, 7419−7424.
(31) Jayawardhana, S.; Rosa, L.; Buividas, R.; Stoddart, P. R.; Juodkazis, S. Light Enhancement in Surface-enhanced Raman Scattering at Oblique Incidence. *Photonic Sens.* **2012**, *2*, 283−288.
(32) Terekhov, S. N.; Kachan, S. M.; Panarin, A. Y.; Mojzes, P. Surface-enhanced Raman Scattering on Silvered Porous Alumina Templates: Role of Multipolar Surface Plasmon Resonant Modes. *Phys. Chem. Chem. Phys.* **2015**, *17*, 31780−31789.
(33) Kang, M.; Zhang, X.; Liu, L.; Zhou, Q.; Jin, M.; Zhou, G.; Gao, X.; Lu, X.; Zhang, Z.; Liu, J. High-Density Ordered Ag@Al_2O_3 Nanobowl Arrays in Applications of Surface-enhanced Raman Spectroscopy. *Nanotechnology* **2016**, *27*, 165304.
(34) Shoute, L. C. T.; Bergren, A. J.; Mahmoud, A. M.; Harris, K. D.; McCreery, R. L. Optical Interference Effects in the Design of Substrates for Surface-enhanced Raman Spectroscopy. *Appl. Spectrosc.* **2009**, *63*, 133−140.
(35) Nayak, D. R.; Bhat, N.; Venkatapathi, M.; Umapathy, S. Impact of Ultrathin Dielectric Spacers on SERS: Energy Transfer between Polarized Charges and Plasmons. *J. Mater. Chem. C* **2017**, *5*, 2123−2129.
(36) Ko, C.-T.; Han, Y.-Y.; Chen, C.-H.; Shieh, J.; Chen, M.-J. Enormous Plasmonic Enhancement and Suppressed Quenching of Luminescence from Nanoscale ZnO Films by Uniformly Dispersed Atomic-layer-deposited Platinum with Optimized Spacer Thickness. *J. Phys. Chem. C* **2013**, *117*, 26204−26212.
(37) Morawiec, S.; Mendes, M. J.; Filonovich, S. A.; Mateus, T.; Mirabella, S.; Águas, H.; Ferreira, I.; Simone, F.; Fortunato, E.; Martins, R.; Priolo, F.; Crupi, I. Broadband Photocurrent Enhancement in a-Si:H Solar Cells with Plasmonic Back Reflectors. *Opt. Express* **2014**, *22*, A1059−A1070.
(38) Mendes, M. J.; Morawiec, S.; Mateus, T.; Lyubchyk, A.; Águas, H.; Ferreira, I.; Fortunato, E.; Martins, R.; Priolo, F.; Crupi, I. Broadband Light Trapping in Thin Film Solar Cells with Self-organized Plasmonic Nano-colloids. *Nanotechnology* **2015**, *26*, 135202.
(39) Li, J.; Cushing, S. K.; Meng, F.; Senty, T. R.; Bristow, A. D.; Wu, N. Plasmon-induced Resonance Energy Transfer for Solar Energy Conversion. *Nat. Photonics* **2015**, *9*, 601−607.
(40) Cushing, S. K.; Li, J.; Meng, F.; Senty, T. R.; Suri, S.; Zhi, M.; Li, M.; Bristow, A. D.; Wu, N. Photocatalytic Activity Enhanced by Plasmonic Resonant Energy Transfer from Metal to Semiconductor. *J. Am. Chem. Soc.* **2012**, *134*, 15033−15041.
(41) Garnett, J. C. M. Colours in Metal Glasses, in Metallic Films, and in Metallic Solutions. II. *Philos. Trans. R. Soc., A* **1906**, *305*, 237−288.
(42) Piredda, G.; Smith, D. D.; Wendling, B.; Boyd, R. W. Nonlinear Optical Properties of a Gold-silica Composite with High Gold Fill Fraction and the Sign Change of Its Nonlinear Absorption Coefficient. *J. Opt. Soc. Am. B* **2008**, *25*, 945−950.
(43) Bohren, C. F.; Huffman, D. R. *Absorption and Scattering of Light by Small Particles*; John Wiley & Sons, 2008.
(44) Heavens, O. S. *Optical Properties of Thin Solid Films*; Courier Corporation, 1991.
(45) Ratsch, C.; Venables, J. A. Nucleation Theory and the Early Stages of Thin Film Growth. *J. Vac. Sci. Technol., A* **2003**, *21*, S96−S109.
(46) Wu, D.-Y.; Ren, B.; Jiang, Y.-X.; Xu, X.; Tian, Z.-Q. Density Functional Study and Normal-mode Analysis of the Bindings and Vibrational Frequency Shifts of the Pyridine−M (M= Cu, Ag, Au, Cu +, Ag+, Au+, and Pt) Complexes. *J. Phys. Chem. A* **2002**, *106*, 9042−9052.

DOI: 10.1021/acs.jpcc.8b01814
J. Phys. Chem. C 2018, 122, 9134−9140